



Article

Microstructure Evolution and Precipitation Behavior in Nb and Nb-Mo Microalloyed Fire-Resistant Steels

Zhengyan Zhang ¹, Zhenqiang Wang ^{2,*}, Zhaodong Li ^{1,*} and Xinjun Sun ¹¹ Department of Structurale Steels, Central Iron and Steel Research Institute, Beijing 100081, China² Key Laboratory of Superlight Materials and Surface Technology, Ministry of Education College of Material Science and Chemical Engineering, Harbin Engineering University, Harbin 150001, China

* Correspondence: wangzhenqiang@hrbeu.edu.cn (Z.W.); lizhaodong@cisri.com.cn (Z.L.)

Abstract: Microstructure evolution and precipitation behaviors before and after tension at elevated temperature of Nb and Nb-Mo microalloyed fire-resistant steels were investigated by scanning electron microscopy and transmission electron microscopy, physical–chemical phase analysis and small-angle X-ray scattering. Results showed that the martensite and austenite (M/A) islands in a rolled state disappeared after tempering, and cementite and a large number of nanometer-sized carbide precipitated. Those nanosized particles were identified as NbC in Nb steel and (Nb, Mo)C in Nb-Mo steel. The precipitation amount of Nb is nearly equal for the two steels in a rolled state. However, after tempering treatment at 600 °C, the precipitation of Nb increased in Nb-Mo steel more obviously than that in Nb steel, indicating that Mo promotes the precipitation of Nb. Correspondingly, the amount of dissolved Nb was reduced, which results in decreased coarsening kinetics of (Nb, Mo)C in Nb-Mo steel as compared with that of NbC in Nb steel.

Keywords: (Nb, Mo)C phase; molybdenum; quantitative analysis; coarsening kinetics



Citation: Zhang, Z.; Wang, Z.; Li, Z.; Sun, X. Microstructure Evolution and Precipitation Behavior in Nb and Nb-Mo Microalloyed Fire-Resistant Steels. *Metals* **2023**, *13*, 112. <https://doi.org/10.3390/met13010112>

Academic Editor: Koh-ichi Sugimoto

Received: 10 December 2022

Revised: 26 December 2022

Accepted: 29 December 2022

Published: 5 January 2023



Copyright: © 2023 by the authors. Licensee MDPI, Basel, Switzerland. This article is an open access article distributed under the terms and conditions of the Creative Commons Attribution (CC BY) license (<https://creativecommons.org/licenses/by/4.0/>).

1. Introduction

In the past several decades, many investigators have focused on developing high-strength steels via adding a certain amount of microalloying elements, such as niobium (Nb), vanadium (V) and titanium (Ti), into steel, which can form carbide and/or carbonitride with C and N [1–17]. Carbide and/or carbonitride play important roles in steel by preventing grain growth during the soaking process, restraining the recrystallization of deformed austenite and exerting precipitation strengthening. It is generally considered that larger precipitation strengthening enhancement can be obtained in Ti- or V-microalloyed steels as compared with that in Nb microalloyed steel, which is mainly due to the difference in atomic weight among them [18]. JFE Holdings, Inc. (JFE)'s work showed that nanometer-sized (Ti, Mo)C with superior thermal stability provided a considerable precipitation strengthening (~300 MPa) in Ti-Mo-containing low-carbon steel [19,20]. Since then, many investigators [21,22] focused on the precipitation behavior of this type of nanometer-sized (Ti, Mo)C in steel. They revealed that the complex (Ti, Mo)C particle with NaCl-type crystal structure shows a fast precipitation kinetics as compared with TiC particles at early stages of the precipitation process, while it exhibited sluggish coarsening kinetics due to the decreased interfacial energy between the ferrite and (Ti, Mo)C particle [23,24].

It is well-known that Nb plays an important role in high-strength low-alloy (HSLA) steels mainly through the significant grain refinement and moderate precipitation hardening. Many works [25,26] suggested that HSLA steels microalloyed with both Nb and Mo exhibit an excellent mechanical property as compared with the conventional ones microalloyed with single Nb, and they have been widely used in pipeline, bridge and fire-resistant building frames. In order to reveal the underlying mechanism of this phenomenon, a series of works were conducted. Lee et al. [27] revealed that HSLA steel

containing both Nb and Mo was attributed to the high density of carbide, resulting from increased nucleation site caused by bainite transformation due to Mo addition. Uemori et al. [28] suggested that Mo restrained the diffusion of Nb atoms into Nb(C,N) from a ferrite matrix by segregating at the Nb(C, N)/ferrite matrix interface in a fire-resistant steel containing Nb and Mo at the elevated temperature, which results in finer precipitates of NbC carbide. However, Enloe et al. [29] found no Mo segregation at the Nb(C, N)/matrix interface in Nb-Mo bearing steel. Although those findings give some explanations of the influence of Mo addition on the MC carbide precipitation and strengthening of Nb bearing HSLA steel, the synergistic effect of Mo and Nb in Nb-Mo bearing HSLA steel are still not completely understood.

Therefore, the aim of the present work is to reveal the influence of Mo on the precipitation and coarsening behavior of MC-type (M = Nb and Mo) carbide in Nb-Mo bearing fire-resistant steel before and after tempering at elevated temperature (ET) 600 °C. Additionally, physical-chemical phase analysis (PCPA) and small-angle X-ray scattering (SAXS) experiments were employed in order to quantitatively analyze the content of precipitated elements and the coarsening behavior of MC particles in steel. In addition, mechanical properties of two low-carbon fire-resistant steels, Nb steel and Nb-Mo steel containing 0.1% Nb and 0.1% Nb-0.19% Mo, were measured to study the effect of Mo on the mechanical properties both at room temperature (RT) and ET (600 °C) and the microstructure evolution from RT to ET (600 °C) as well.

2. Materials and Methods

The two experimental steels were prepared by vacuum-induction melting in a 50 kg vacuum-induction furnace. The smelted steels were casted as a cylindrical ingot with a diameter of about 140 mm and a length of about 300 mm. The ingots were heated to 1200 °C in soaking furnace for 2 h and then forged. The beginning forging temperature was not lower than 1150 °C, and the finishing forging temperature was not lower than 950 °C. After repeated forging by the forging hammer, the cylindrical ingots were forged into a rectangular billet with the size of 110 mm in width and 60 mm in thickness; finally, they were cut into 120 mm long square billets for rolling. The forging reduction rate is about 57%. After 1 h soaking at 1220 °C (because the solution temperature of NbC in Nb and Nb-Mo steels are 1145 °C and 1167 °C, respectively, calculated by Thermo-Calc Software (TCFE12 database)), the tested steels were rolled in the region through the recrystallization region above ~950 °C to the non-recrystallization region. The finish-rolling temperature is about 880 °C, followed by laminar cooling (the cooling rate ≥ 15 °C/s) to about 400 °C. Then, the steels were cooled down to room temperature by air quenching. During the rolling process, the rolling reduction per pass is about 20% and the finish-rolling thickness of the steel strip is 12 mm. Figure 1 shows the schematic illustration of the rolling process. In order to study the precipitation behavior of experimental steels at 600 °C, the hot-rolled steel plate was tempered at 600 °C for 15 min and 60 min. The chemical compositions of the as-rolled steels were determined by optical emission spectrometry, as given in Table 1. The chemical compositions of two steels are only different in Mo. One has no Mo addition, and the other one contains 0.19 wt % Mo. Here, the two steels are designated as Nb and Nb-Mo steel, respectively. In the two steels, the C content is designed to be low not only to make sure that all Nb can dissolve, but also ensure a good weldability of steel. A small amount of Ti (~0.015 wt %) was added to fix nitrogen by forming TiN, which can prevent the initial austenite grain growth during the soaking process. Meanwhile, in order to increase the hardenability, moderate Mn and B were alloyed.

Dog-bone-shaped tensile specimens were machined with a gauge length of 40 mm and a diameter of 8 mm. Tensile tests (along the transverse direction) both at RT and ET 600 °C were conducted following the Chinese standards GB/T228-2010 and GB/T4338-2006, respectively. Meanwhile, the investigation of SEM, TEM and EBSD for rolled steels and the screw thread part of ET (600 °C) tensile specimens were also observed. This is mainly because there is no effect of strain on the screw thread part.

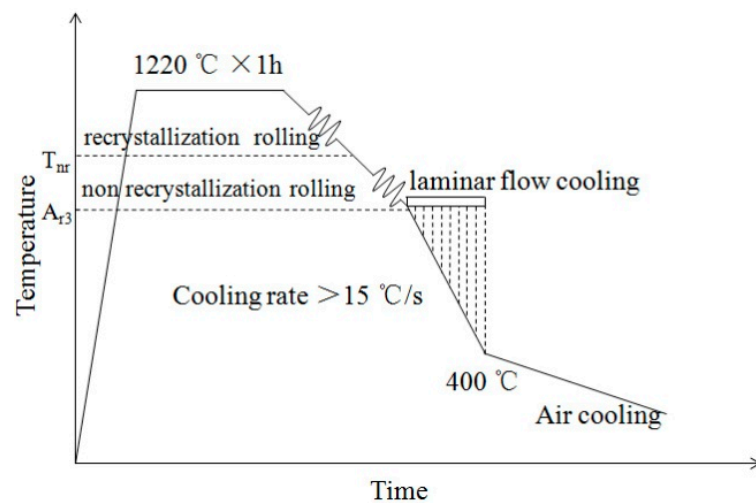


Figure 1. Schematic diagram of the TMCP process.

Table 1. Chemical compositions of the investigated steels (wt.%).

Steel	C	Mn	P	S	Si	Mo	Ti	Nb	N	Al	B	Fe
Nb	0.036	1.35	0.0034	0.0057	0.024	-	0.010	0.10	~0.004	0.012	0.0012	Bal.
Nb-Mo	0.042	1.38	0.0040	0.0060	0.016	0.19	0.015	0.10	~0.004	0.014	0.0010	Bal.

The microstructures of the specimens from the two strips in a cross-section along the rolling direction were mainly characterized via S-4300 cold-field emission scanning electron microscope (SEM, HITACHI, Tokyo, Japan) and Tecnai F20 transmission electron microscope (TEM, FEI Company, Hillsboro, OR, USA) equipped with a nanometer probe energy dispersive spectrometer (EDS, FEI Company, Hillsboro, OR, USA), respectively. The samples were mechanically polished and then etched in 3% nital solution for about 15 s for SEM observation. The thin foils were prepared with about 35 μm in thickness for TEM observation after mechanically thinning and twin-jet polishing in a solution of 6% perchloric acid and 94% alcohol at about $-25\text{ }^\circ\text{C}$. Electron back-scatter diffraction (EBSD, Oxford Instruments, Abindon, Oxfordshire, UK) measurements were carried out in order to quantify the effective grain size and the grain boundary density of two steels. The grain boundary density can be defined as $\rho = L_{GB}/A$, where ρ is density of grain boundary, L_{GB} is total length of grain boundary and A is the total area scanned by EBSD. For EBSD measurement, the test samples were mechanically grinded and polished on the conventional grinding papers and electro-polished using 10% perchloric acid +90% acetic acid at 20 V at room temperature for 12 s. The step size was 0.2 μm , and total area scanned was $100 \times 100\ \mu\text{m}^2$ for each sample. Additionally, the data obtained were analyzed by Channel 5 software. The carbon extraction replica technique was employed to identify the morphology and size distribution of precipitates in two steels.

Physical–chemical phase analysis (PCPA) and X-ray diffraction (XRD, PANalytical B.V., Almelo, The Netherlands) were employed to qualitatively and quantitatively analyze the precipitates in tested steel. Additionally, the rolled experimental steels were tempered at 600 $^\circ\text{C}$ for 15 min and 60 min, respectively, in order to simulate precipitation in fire-resistant steel at elevated temperature. The elemental mass fraction of the MC precipitate in tested steel was determined by PCPA. The lattice structure of the precipitates obtained by electrolysis were identified by XRD within the 2θ range of $20\text{--}90^\circ$. The particle size distribution was acquired through small-angle X-ray scattering (SAXS, Anton Paar, Graz, Austria) goniometer with Co $K\alpha$ at 30 kV and 30 mA. The detailed methods of PCPA and SAXS can be found in reference [30].

3. Results and Discussion

3.1. Mechanical Property

Tensile properties of the two tested steels both at RT and ET (600 °C) are listed in Table 2. The yield strengths at RT are 511 MPa and 550 MPa for Nb steel and Nb-Mo steel, respectively, and 315 MPa and 395 MPa at 600 °C, respectively. This indicates that Mo addition increases the strength both at RT and 600 °C. In addition, the fire resistance (FR), which is usually expressed as $R_{p0.2}(ET)/R_{p0.2}(RT)$, should be not less than 2/3 [31]. The FR of Nb steel is 0.62, which is less than 2/3, but it is 0.72 for Nb-Mo steel, which is higher than 2/3. This indicates that Mo addition could increase the FR, which meets the standard of FR.

Table 2. Mechanical properties of two tested steels.

Steels	R_m /MPa	$R_{p0.2}$ /MPa	A/%	R_m (600 °C)/MPa	$R_{p0.2}$ (600 °C)/MPa	$R_{p0.2}$ (600 °C)/ $R_{p0.2}(RT)$
Nb	618	511	23	368	315	0.62
Nb-Mo	642	550	19	450	395	0.72

3.2. Microstructural Evolution

The microstructures of both the as-rolled Nb and Nb-Mo steels, which are shown in Figure 2a,b, mainly consisted of polygonal ferrite and granular bainite. Under the continuous cooling process after finish rolling, the carbon in steel would concentrate into untransformed austenite when γ/α transformation takes place. Then, a part of untransformed austenite transformed into martensite, and the other part of it was still retained at the lower temperature as residual austenite, which consisted of the island-style phase named martensite/austenite (M/A) islands, as shown in Figure 2a,b. Those M/A islands are distributed on the matrix and white-etched particles with the size $\sim 1 \mu\text{m}$ (inserted in Figure 2b). Furthermore, there is a small amount of pearlite in the as-rolled Nb steel (inserted in Figure 2a, while not in the as-rolled Nb-Mo steel). This may be mainly due to the Mo addition, which may increase the hardenability of steel and thus restrain pearlite transformation. Meanwhile, the microstructures of ET (600 °C) tensile specimens were also observed, as shown in Figure 2c,d. A large number of white-etched particles are distributed on the ferrite matrix (inserted in Figure 2d). However, those particles' morphology are different from the M/A islands and mainly distribute on ferrite grain boundaries (inserted in Figure 2d).

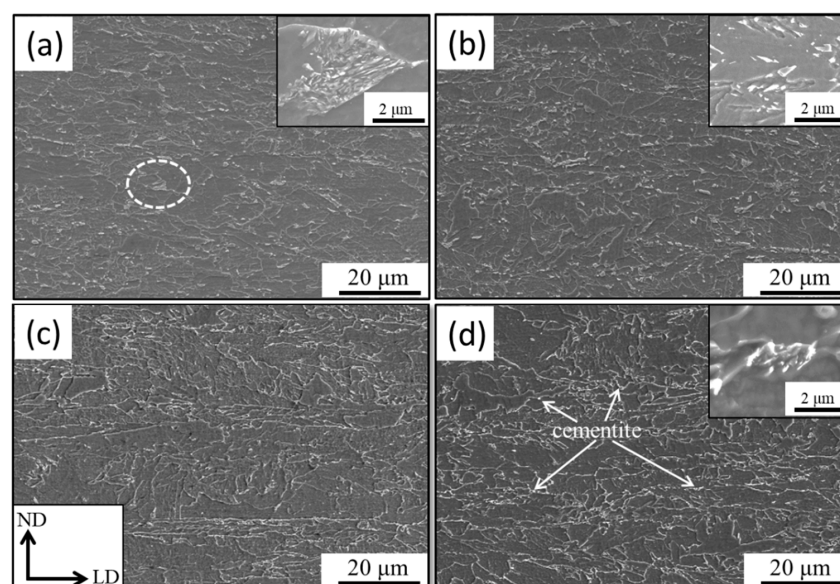


Figure 2. SEM images of as-rolled specimens for (a) Nb and (b) Nb-Mo steel, respectively, and 600 °C tensile specimens for (c) Nb and (d) Nb-Mo steel, respectively. (ND represents normal direction, and LD represents rolling direction).

The fine microstructure characterization of Nb-Mo steel observed by TEM is shown in Figure 3. The typical substructural characteristic of granular bainite in as-rolled Nb-Mo steel was composed of elongated lath ferrite with high density of dislocations (marked by arrows in Figure 3a). Figure 3b displayed the feature of an M/A island with the size of $\sim 0.6 \mu\text{m}$, which was located on the ferrite grain boundary. Figure 3c exhibited the precipitates which were located on the ferrite grain boundary in the ET tensile specimen and the corresponding diffraction spot (Figure 3d). Those precipitates are identified as cementites.

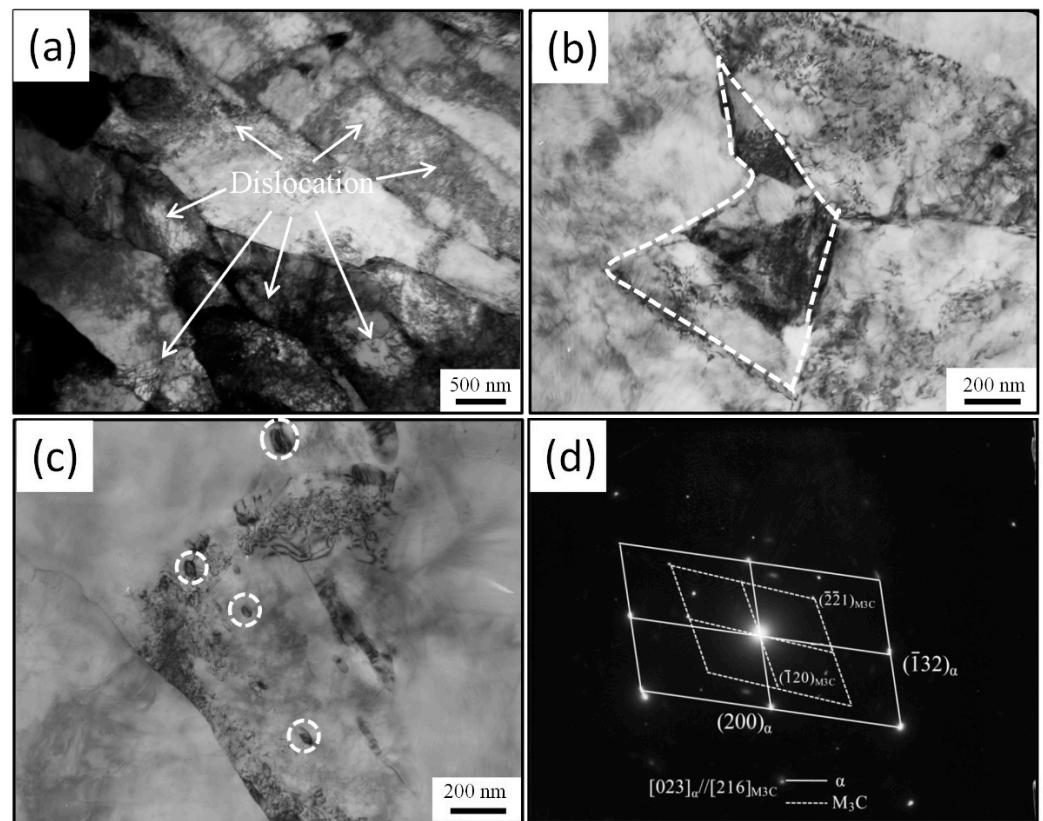


Figure 3. TEM images of the microstructure of Nb-Mo steel: (a) ferrite lath of granular bainite and dislocation in it and (b) an M/A island in rolled samples, (c) cementite in 600 °C tensile specimen and (d) the corresponding diffraction spot of particles in (c).

3.3. Grain Boundaries Misorientation

The EBSD images exhibiting the grain boundaries' misorientation angle distribution of the microstructure of the as-rolled Nb and Nb-Mo steels before and after ET tension are shown in Figure 4. The mean effective grain sizes of ferrite ($\theta \geq 15^\circ$, indicated as black lines) of as-rolled Nb steel before and after ET tension were 8.3 and 8.1 μm , respectively, and 7.2 and 6.9 μm for steels microalloyed with Nb-Mo. It is seen that the effective grain size of ferrite in as-rolled Nb and Nb-Mo steels had negligible change before and after ET tension. However, by adding Mo, the effective grain size of ferrite in both the as-rolled and ET specimens decreased. This may be attributed to the effect of Mo addition on the inhibiting of the deformed austenite from recrystallization during the non-recrystallization rolling process. On the one hand, Mo in solid solution could restrain the recrystallization of deformed austenite. On the other hand, MC-type carbides that were precipitated in austenite of Nb-Mo steel exhibited finer and denser as compared with those of Nb steel [32]. Such fine carbide precipitated by deformation, inducing in austenite, would significantly restrain austenite recrystallization [33].

Meanwhile, the total grain boundary density of as-rolled Nb and Nb-Mo steels before and after ET tension were analyzed by means of EBSD, as shown in Figure 5. It can be seen that low-angle boundaries ($2^\circ \leq \theta \leq 15^\circ$, indicated as red lines in Figure 4) which

are mainly composed of dislocations have the larger grain boundary density, namely, 0.68 and $0.87 \mu\text{m}^{-1}$ for as-rolled Nb steels before and after tension at ET, respectively. After adding Mo, these values are 0.77 and $0.99 \mu\text{m}^{-1}$ for as-rolled Nb-Mo steels before and after tension at ET, respectively. From those findings, it can be seen that the low-angle boundary density of specimens undergoing tension at ET was slightly larger than that of as-rolled steel, regardless of Nb and Nb-Mo steels. This may be mainly due to the slighter plastic deformation taking place during tension, which introduces more dislocations. Furthermore, it is seen that the low-angle boundary density increased after microalloying Mo in Nb-Mo steel as compared with that of Nb steel. This indicated that Mo inhibited the annihilation of dislocations, which is consistent with the result of [27].

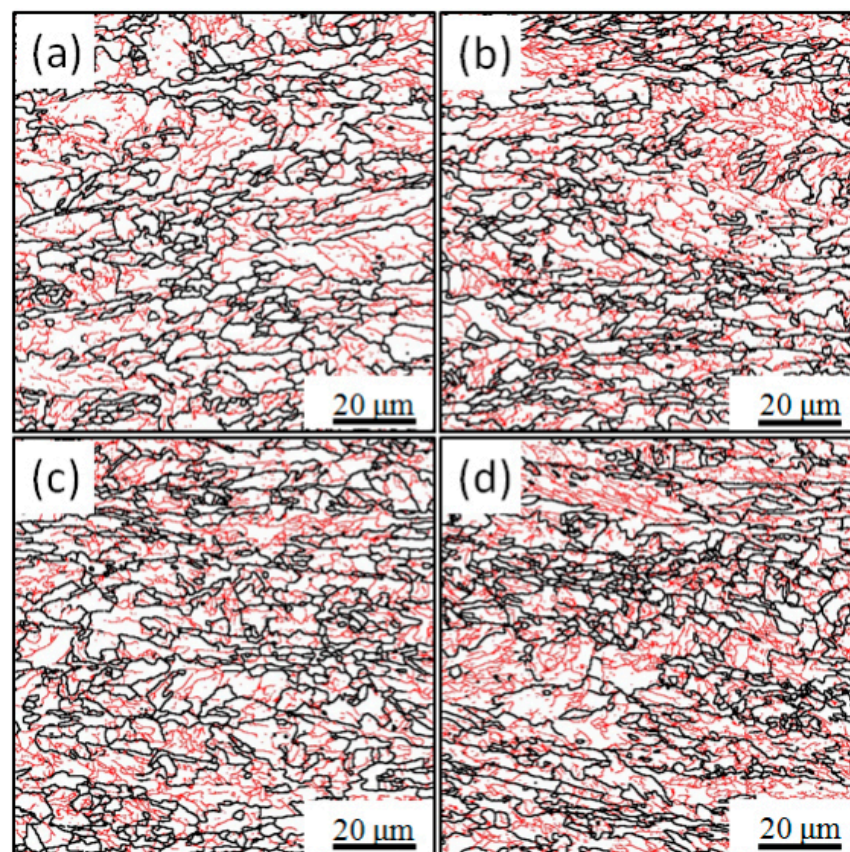


Figure 4. The grain boundaries misorientation angle distribution of the rolled samples for (a) Nb and (b) Nb-Mo steel, and the specimens of tensile test at $600 \text{ }^{\circ}\text{C}$ for (c) Nb and (d) Nb-Mo steels. Black and red lines indicate the ferrite grain boundary ($\theta \geq 15^{\circ}$) and low-angle boundary ($2^{\circ} \leq \theta \leq 15^{\circ}$), respectively.

3.4. Precipitation of MC-Type Carbide

The TEM micrographs of precipitates in different specimens are shown in Figure 6. All the precipitates with a size of less than 10 nm exhibited a spherical shape and uniformly distributed on the carbon films. The EDS results in Figure 6 show that the chemical compositions of the precipitates were Nb and C (in Figure 6e) in Nb steel and Nb, Mo and C (in Figure 6f) in Nb-Mo steel (the peaks of Cu on EDS spectrum are from Cu grid used to support carbon replica film), indicating the precipitates are NbC in Nb steel and (Nb, Mo)C in Nb-Mo steel. In addition, it is noted that the number density of precipitate in rolled specimens (Figure 6a,b) is obviously lower than that in $600 \text{ }^{\circ}\text{C}$ tensile specimens (Figure 6c,d) due to the fast cooling process after finishing rolling, which can restrain the precipitation during cooling process. Furthermore, from Figure 6, it is seen that Mo addition evidently promoted the precipitates of carbides, especially after tempering. It can be found that the carbides in Nb-Mo steel after tempering are the finest and densest compared to those in the other three specimens.

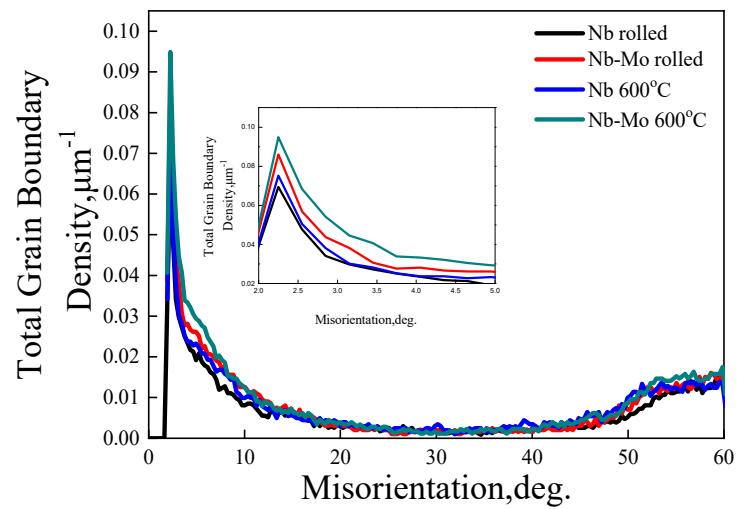


Figure 5. Total grain boundary density distribution of rolled samples and 600 °C tensile specimens for Nb and Nb-Mo steels. The insert figure is the enlarged grain boundary density distribution in the misorientation range of 2.0–5.0°.

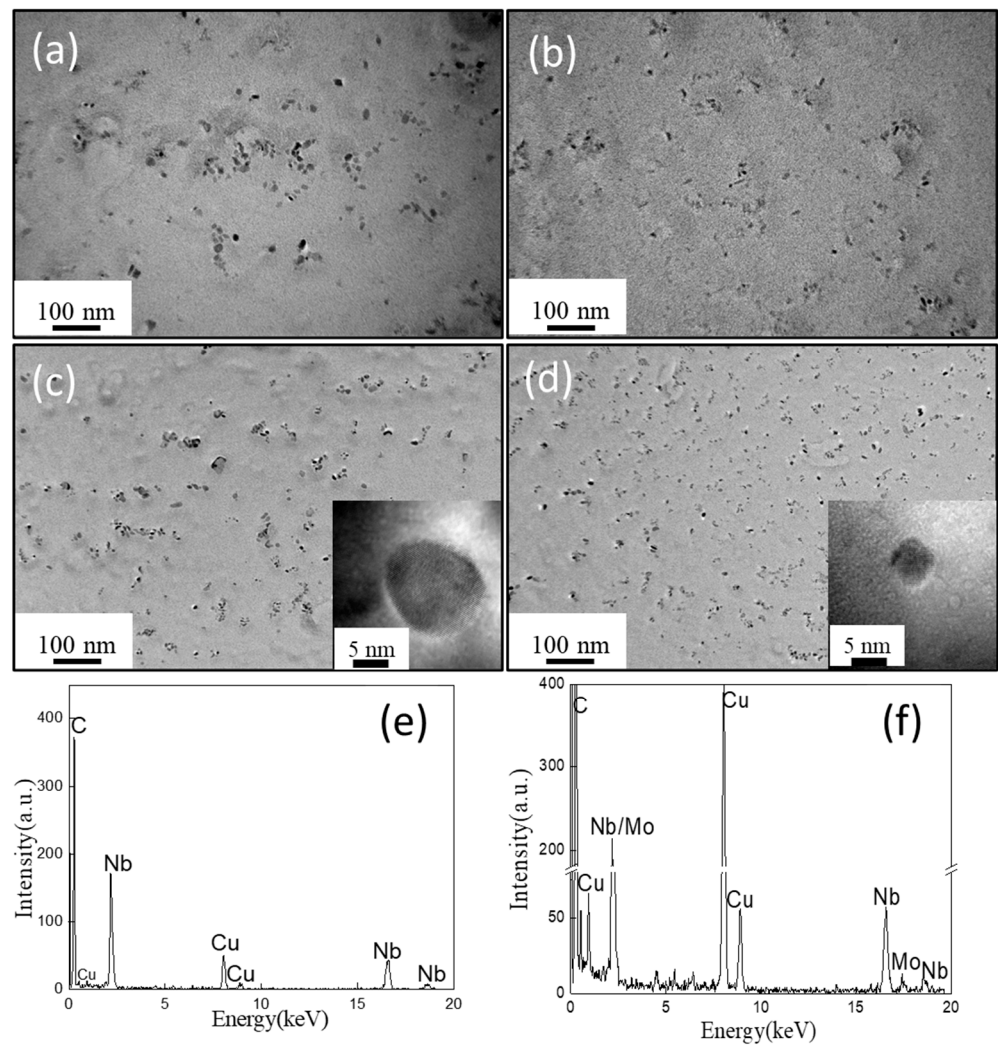


Figure 6. TEM micrographs showing the precipitation characteristics of (a) Nb-R, (b) Nb-Mo-R, (c) Nb-T and (d) Nb-Mo-T steels and the corresponding EDS, (e) for (c) and (f) for (d) (R denotes the rolling condition, and T stands for tempering condition).

Figure 7 shows a high-resolution TEM of a particle (Nb, Mo)C that precipitated from Nb-Mo steel after ET tension. It can be seen from Figure 7a that the particle size is about 7.3 nm, and the diffraction pattern after Fourier transformation shows that the particle is characterized by an FCC structure. The interplanar spacing (001) of the particle was determined to be 0.4391 nm (Figure 7b), which was slightly smaller than the spacing of the (001) planes of NbC, $d_{001} = 0.4477$ nm [26]. This is mainly because the radius of the Mo atom is smaller than the radius of Nb atom; when Mo enters into the sublattice of Nb in NbC, the lattice parameter will be reduced.

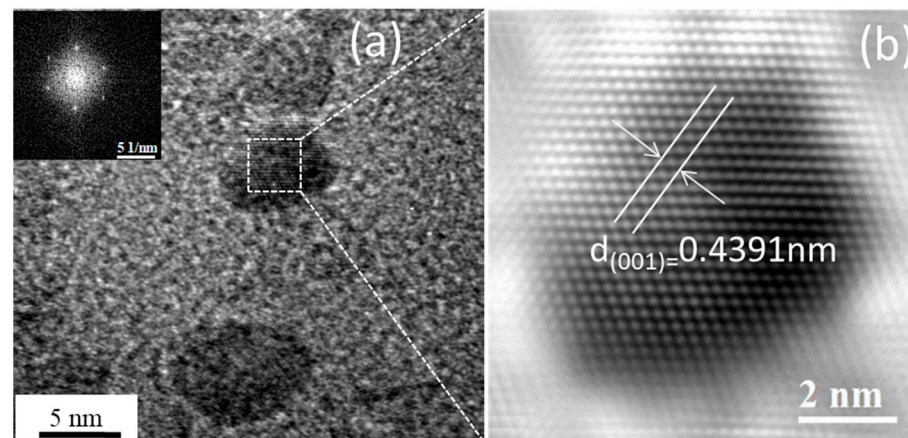


Figure 7. High-resolution image of a (Nb, Mo)C particle (a) and Inverse Fast Fourier Transform (IFFT) of area marked by a white-line frame on the this carbide particle (b).

The precipitates electrolytically extracted from four different specimens by means of PCPA were confirmed with XRD diffraction spectrum, as shown in Figure 8, from which it can be seen that the precipitates are mainly composed of Fe_3C and Nb carbides. There is only a weaker peak of TiN because of the small content of Ti and N in steels.

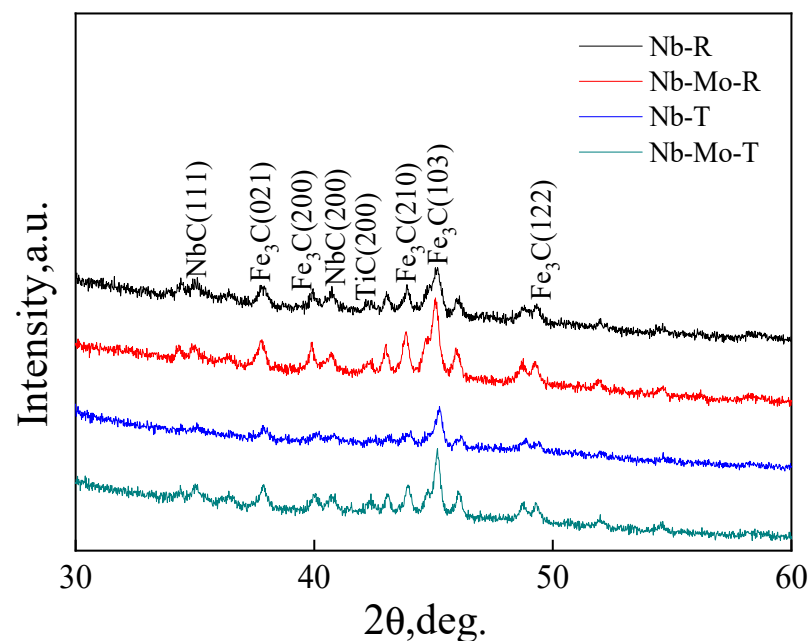


Figure 8. XRD patterns of precipitates electrolytically extracted from Nb and Nb-Mo steels before and after tension at 600 °C.

The quantitative result of MC-type carbides analyzed by PCPA test are shown in Table 3. Since the Ti and N can easily form TiN at high temperatures during the soaking

process, all Ti in steel can be assumed to be consumed by N. Consequently, the MC-type precipitates analyzed here did not include the TiN. From Table 3, it can be seen that the precipitation ratios of Nb are 25% and 26% in as-rolled Nb and Nb-Mo steels, respectively, and 54% and 64% in Nb and Nb-Mo steels tempered at 600 °C for 15 min, respectively (marked Nb-T and Nb-Mo-T for Nb and Nb-Mo steels, respectively). This implies that the precipitation of Nb is restrained during the process of fast cooling after finish rolling. Furthermore, the amount of Nb precipitated in Nb-Mo steel is higher than in that of Nb steel after tempering, indicating that Mo could promote the precipitate of Nb, which is consistent with the results of TEM observation.

Table 3. Quantitative results of phase analysis.

Steels	Number of Elements in MC wt %		Precipitate Ratio of Nb and Mo, %	
	Nb	Mo	Nb	Mo
Nb-R	0.025	-	25	-
Nb-Mo-R	0.026	0.003	26	1.6
Nb-T	0.054	-	54	-
Nb-Mo-T	0.064	0.024	64	13
Nb-T2	0.076	-	76	-
Nb-Mo-T2	0.078	0.028	78	14

However, in the rolled state, the amounts of Nb in Nb and Nb-Mo steel are almost equal. This is mainly because of the faster cooling rate after finish rolling, resulting in insufficient precipitation of Nb during limited time of cooling. This precipitation behavior depending on the TMCP adopted in this work plays an important role in controlling the appropriate strength of steel. That is, the yield ratio should not be as high as fire-resistant steel for construction buildings, so the precipitate of Nb should be restrained to ensure the lower precipitation strengthening. However, when it bursts into flames, the precipitation of Nb carbides is very important to compensate for the decreased strength of steel. Especially, those particles of Nb carbides with the size of smaller than 10 nm that precipitated from ferrite will play a significant role in precipitation strengthening.

From the above analysis, it can be seen that the addition of Mo can promote bainite transformation; increase the low-angle boundaries density, namely, dislocation density of steel; and refine the effective grain size; so, it can improve the strength of as rolled steel. When it comes to improving the elevated temperature strength of tested steel, it is mainly because the addition of Mo can promote the carbide precipitation of Nb and inhibit its coarsening.

The mechanism of Mo addition that promotes the precipitation of NbC in ferrite of Nb-Mo bearing steel was investigated in our previous work [25]. It was suggested that the incorporation of Mo into NbC lattice decreased the lattice parameter of the precipitated NbC, resulting in a decrease of the mismatch between NbC and the ferrite matrix. So, it could decrease the interfacial energy of NbC/ferrite matrix, which was the main reason for promoting the precipitation of NbC in ferrite at the early stage of the precipitation process. However, the influence of Mo on the coarsening resistance of NbC has not been discussed deeply yet.

In order to investigate the coarsening behaviors of MC-type carbide, two as-rolled Nb and Nb-Mo steels were tempered at 600 °C for a longer time, i.e., 60 min (marked Nb-T2 and Nb-Mo-T2 for Nb and Nb-Mo steels, respectively). Additionally, the MC-type precipitates were electrolytically extracted by PCPA tests. The size distribution of MC-type precipitates in different specimens, ranging from 0 to 300 nm, were measured by means of SAXS, as shown in Figure 9. The carbides with the size of less than 10 nm can be considered as precipitation in ferrite, and the mass percent of precipitates in ferrite are 16.8%, 22.9%, 24.8%, 32.1%, 13.3% and 43.6% in the specimens of Nb-R, Nb-Mo-R, Nb-T, Nb-Mo-T, Nb-T2 and Nb-Mo-T2, respectively. It is noted that those particles within the size of 10 nm increased after tempering 15 min at 600 °C, and Mo addition promoted the

precipitation of MC-typed carbides. When the tempering time reached 60 min, the mass percent of particles within the size of 10 nm in Nb steel decreased, while those increased in Nb-Mo steel. This implies that Mo addition is favorable to the coarsening resistance of carbide precipitated in ferrite.

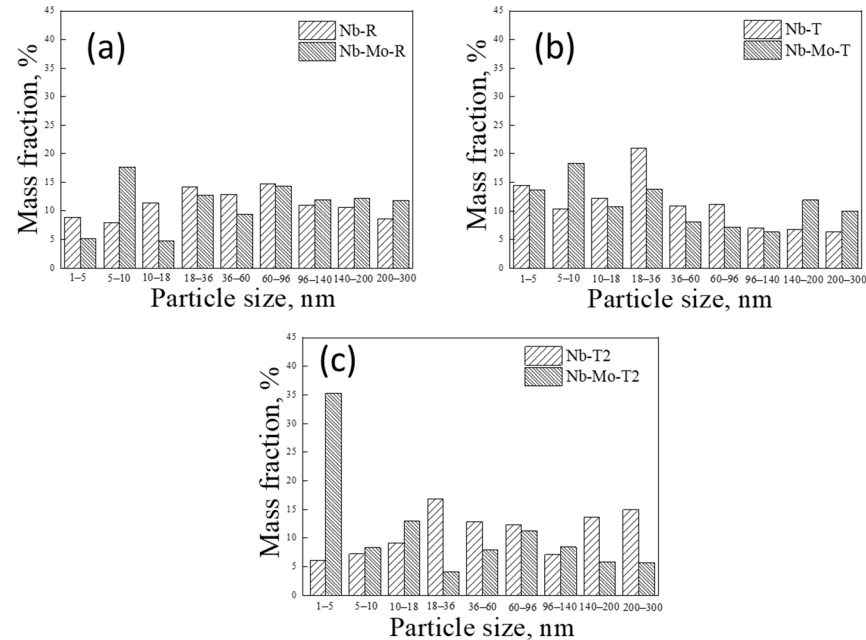


Figure 9. Size distribution of MC type precipitates in (a) rolled samples for Nb and NbMo steels and (b) Nb and Nb-Mo steels tempered at 600 °C for 15 min of, and (c) Nb and Nb-Mo steels tempered at 600 °C for 60 min, respectively.

According to Ostwald's ripening theory:

$$d_t^n - d_0^n = \frac{K}{RT} V_m^2 C D \sigma t \quad (1)$$

where d_t is average particle size at given time (t), d_0 is initial average particle size, n is 3 for volume diffusion controlled coarsening, k is a constant, V_m is the molar volume of the precipitate, C is the concentration of the solute in the ferrite matrix that is in equilibrium with the precipitate, D is the diffusivity of the solute, σ is the interfacial energy per unit area between precipitate and ferrite matrix, R is universal constant and T is absolute temperature. The coarsening rate was controlled by the C , D and σ rather than the other constants such as V_m , etc. Since the activation energy of the diffusion of interstitial atoms is much smaller than that of a substitutional element, the controlled element of diffusion during the coarsening process is considered to be the substitutional element Nb in Nb steel and Nb or Mo in Nb-Mo steel. Yong [18] holds that the controlled element of diffusion of the ternary carbide, such as (Nb, Mo)C, during the coarsening process is determined by the product of CD of substitutional element Nb and Mo in solution. Additionally, the element with a smaller product of CD can be determined the controlled element of diffusion. In this paper, according to the PCPA results, it noted that the amount of Nb and Mo in solution in the ferrite matrix decreased with the increase in tempering time at 600 °C; especially, when the tempering time reached 60 min, most of the Nb was precipitated. Additionally, Mo addition accelerated the precipitation of Nb in Nb-Mo steel as compared with the Nb steel. In addition, Equations (2) and (3) [18] exhibited the diffusion coefficients of Nb and Mo atoms in ferrite, respectively, from which we can know that the diffusion coefficients of Nb are about two times larger than those of Mo at 600 °C. Thus, the product of CD for Nb and Mo atoms can be calculated after tempering 15 min at 600 °C and are $1.5080715 \times 10^{-5} \text{ cm}^2 \text{ s}^{-1}$ and $4.28239 \times 10^{-5} \text{ cm}^2 \text{ s}^{-1}$ for Nb and Mo atoms, respectively.

The value of CD of Nb is smaller than that of Mo, which indicated that the controlled element of diffusion during the coarsening stage can be controlled by the Nb atom.

$$D_{Nb} = 50.2 \times \exp(-252000/RT) \quad (2)$$

$$D_{Mo} = 1.3 \times \exp(-229000/RT) \quad (3)$$

On the one hand, the lower interfacial energy between (Nb, Mo)C and ferrite matrix, due to a certain amount of Mo incorporating into NbC lattice [25], also contributed to the decrease in the coarsening rate.

4. Conclusions

Microstructure evolution and precipitation behaviors before and after tempering of Nb and Nb–Mo microalloyed fire-resistant steels were investigated, and the influence of Mo on the precipitation and coarsening behavior of Nb carbides during tempering was studied. The summaries are as follows:

- Martensite and austenite (M/A) islands in Nb and Nb–Mo microalloyed fire-resistant steel disappear after elevated temperature tension, and cementite and nanometer-sized carbide precipitated.
- The precipitation amount of Nb is nearly equal for the two steels in rolled state; it increased in Nb–Mo steel more obviously than that in Nb steel after tempering treatment at 600 °C, indicating that Mo promotes the precipitation of Nb.
- The controlled element of diffusion during the coarsening stage of the (Nb, Mo)C particle can be determined as the Nb atom in Nb–Mo steel, and the amount of dissolved Nb was reduced, which results in decreased coarsening kinetics of (Nb, Mo)C in Nb–Mo steel as compared with that of NbC in Nb steel.

Author Contributions: Resources, data curation and writing—original draft preparation, Z.Z.; funding acquisition and writing—review and editing, Z.W.; writing—original draft preparation, investigation, funding acquisition and writing—review, Z.L.; investigation and formal analysis, X.S. All authors have read and agreed to the published version of the manuscript.

Funding: This research was funded by the National Key Research and Development Program of China (Grant No. 2022YFB3706401), the National Natural Sciences Foundation of China (Grant No. 52001084), Outstanding Youth Fund of Heilongjiang Natural Science Foundation (Grant YQ2022E010) and the Central University Foundation of Harbin Engineering University (Grant No. GK2100260329).

Data Availability Statement: The data in this paper are obtained from experiments. All data generated in this study are included in this manuscript.

Conflicts of Interest: The authors declare no conflict of interest.

References

1. Yong, Q.L. *Microalloyed Steels—Physical and Mechanical Metallurgy, Metall*; Industry Press: Beijing, China, 1989.
2. Xiong, Z.P.; Timokhina, I.; Pereloma, E. Clustering, nano-scale precipitation and strengthening of steels. *Prog. Mater. Sci.* **2021**, *118*, 100764. [[CrossRef](#)]
3. Yoo, J.; Jo, M.C.; Bian, J.B.; Sohn, S.S.; Lee, S. Effects of Nb or (Nb + Mo) alloying on Charpy impact, bending, and delayed fracture properties in 1.9-GPa-grade press hardening steels. *Mater. Charact.* **2021**, *176*, 111133. [[CrossRef](#)]
4. Mao, X.P.; Huo, X.D.; Sun, X.J. Strengthening mechanisms of a new 700MPa hot rolled Ti-microalloyed steel produced by compact strip production. *J. Mater. Proc. Tech.* **2010**, *210*, 1660–1666. [[CrossRef](#)]
5. Wu, W.; Cai, M.; Zhang, Z.; Tian, W.; Pan, H. Elevated Temperature Tensile Behavior of a Nb–Mo Microalloyed Medium Mn Alloy under Quasistatic Loads. *Metals* **2022**, *12*, 442. [[CrossRef](#)]
6. Wang, Z.Q.; Huo, D.S.; Zhou, Y.Y.; Sui, G.Y.; Jiang, F.C. Effect of Tungsten Addition on Continuous Cooling Transformation and Precipitation Behavior of a High Titanium Microalloyed Steel. *Metals* **2022**, *12*, 1649. [[CrossRef](#)]
7. Wang, Z.Q.; Yong, Q.L.; Sun, X.J. An analytical model for the kinetics of strain-induced precipitation in titanium micro-alloyed steels. *ISIJ Int.* **2012**, *52*, 1661–1669. [[CrossRef](#)]

8. Claesson, E.; Magnusson, H.; Kohlbrecher, J.; Thuvander, M.; Lindberg, F.; Andersson, M.; Hedström, P. Carbide Precipitation during Processing of Two Low-Alloyed Martensitic Tool Steels with 0.11 and 0.17 V/Mo Ratios Studied by Neutron Scattering, Electron Microscopy and Atom Probe. *Metals* **2022**, *12*, 758. [[CrossRef](#)]
9. Park, D.B.; Huh, M.Y.; Shim, J.H.; Suh, J.Y.; Lee, K.H.; Jung, W.S. Strengthening mechanism of hot rolled Ti and Nb microalloyed HSLA steels containing Mo and W with various coiling temperature. *Mater. Sci. Eng. A* **2013**, *560*, 528–534. [[CrossRef](#)]
10. Liu, C.Q.; Xiong, F.; Wang, Y.; Cao, Y.X.; Liu, X.B.; Xue, Z.L.; Peng, Q.C.; Peng, L.S. Strengthening mechanism and carbide precipitation behavior of Nb-Mo microalloy medium Mn steel. *Metals* **2021**, *14*, 7461. [[CrossRef](#)]
11. Kim, Y.W.; Song, S.W.; Seo, S.J.; Hong, S.J.; Lee, C.S. Development of Ti and Mo micro-alloyed hot-rolled high strength sheet steel by controlling thermomechanical controlled processing schedule. *Mater. Sci. Eng. A* **2013**, *565*, 430–438. [[CrossRef](#)]
12. Zhang, Y.; Yu, B.; Zhang, J.; Du, Y.; Wang, X.; Wu, H.; Gao, X.H.; Du, L.X. Microstructure, Mechanical Properties, and Fish-Scaling Resistance of a Ti-Nb Microalloyed Hot-Rolled Enamel Steel. *Metals* **2022**, *12*, 1970. [[CrossRef](#)]
13. Huang, H.H.; Yang, G.W.; Zhao, G.; Mao, X.P.; Gan, X.L.; Yin, Q.L.; Yi, H. Effect of Nb on the microstructure and properties of Ti-Mo microalloyed high-strength ferritic Steel. *Mater. Sci. Eng. A* **2018**, *736*, 148–155. [[CrossRef](#)]
14. Yu, Q.B.; Wang, Z.D.; Liu, X.H.; Wang, G.D. Effect of microcontent Nb in solution on the strength of low carbon steels. *Mater. Sci. Eng. A* **2004**, *379*, 384–390. [[CrossRef](#)]
15. Wang, Z.H.; Hui, W.J.; Chen, Z.; Zhang, Y.J.; Zhao, X.L. Effect of vanadium on microstructure and mechanical properties of bainitic forging steel. *Mater. Sci. Eng. A* **2020**, *771*, 138653. [[CrossRef](#)]
16. Fang, F.; Hu, X.; Zhou, L.; Jiang, J. Effect of vanadium on microstructure and property of pearlitic steel wire. *Mater. Res. Innov.* **2015**, *19*, 394–396. [[CrossRef](#)]
17. Chen, C.Y.; Yang, J.R.; Chen, C.C.; Chen, S.F. Microstructural characterization and strengthening behavior of nanometer sized carbides in Ti-Mo microalloyed steels during continuous cooling process. *Mater. Charact.* **2016**, *114*, 18–29. [[CrossRef](#)]
18. Yong, Q.L. *Secondary Phases in Steels, Metall*; Industry Press: Beijing, China, 2006.
19. Funakawa, Y.; Shiozaki, T.; Tomita, K.; Yamamoto, T.; Maeda, E. Development of High Strength Hot-rolled Sheet Steel Consisting of Ferrite and Nanometer-sized Carbides. *ISIJ Int.* **2004**, *44*, 1945–1951. [[CrossRef](#)]
20. Shimizu, T.; Funakawa, Y.; Kaneko, S. High Strength Steel Sheets for Automobile Suspension and Chassis Use-High Strength Hot-Rolled Steel Sheets with Excellent Press Formability and Durability for Critical Safety Parts. *JFE Tech. Rep.* **2004**, *4*, 25–31.
21. Hu, B.H.; Cai, Q.W.; Wu, H.B. Influence of Mo on Growth and Coarsening of Nanometer-sized Carbides in Low-alloy Ferritic Steels Containing Ti. *J. Iron Steel Res. Int.* **2014**, *21*, 878–885. [[CrossRef](#)]
22. Timokhina, I.; Miller, M.K.; Wang, J.T. On the Ti-Mo-Fe-C atomic clustering during interphase precipitation in the Ti-Mo steel studied by advanced microscopic techniques. *Mater. Des.* **2016**, *111*, 222–229. [[CrossRef](#)]
23. Dong, H.; Chen, H.; Khorasgani, A.R.; Zhang, B.; Zhang, Y.J.; Wang, Z.Q.; Zhou, X.S.; Wang, W.; Wang, H.R.; Li, T.; et al. Revealing the influence of Mo addition on interphase precipitation in Ti-bearing low carbon steels. *Acta Mater.* **2022**, *223*, 117475. [[CrossRef](#)]
24. Wang, Y.Q.; Clark, S.J.; Cai, B.; Venero, D.A.; Yan, K.; Gorley, M.; Surrey, E.; McCartney, D.G.; Sridhar, S.; Lee, P.D. Small-angle neutron scattering reveals the effect of Mo on interphase nano-precipitation in Ti-Mo micro-alloyed steels. *Scr. Mater.* **2020**, *174*, 24–28. [[CrossRef](#)]
25. Zhang, Z.Y.; Li, Z.D.; Yong, Q.L.; Sun, X.J.; Wang, Z.Q.; Wang, G.D. Precipitation behavior of carbide during heating process in Nb and Nb-Mo microalloyed steels. *Acta Metall. Sin.* **2015**, *51*, 315–324.
26. Jang, J.H.; Lee, C.H.; Heo, Y.U. Stability of (Ti, M)C (M = Nb, V, Mo and W) carbide in steels using first-principles calculations. *Acta Mater.* **2012**, *60*, 208–217. [[CrossRef](#)]
27. Lee, W.B.; Hong, S.G.; Park, C.G.; Kim, K.H.; Park, S.H. Influence of Mo on precipitation hardening in hot rolled HSLA steels containing Nb. *Scr. Mater.* **2000**, *43*, 319–324. [[CrossRef](#)]
28. Uemori, R.; Chijiwa, R.; Tamehiro, H.; Morikawa, H. AP-FIM study on the effect of Mo addition on microstructure in Ti-Nb steel. *Appl. Surf. Sci.* **1994**, *76*, 255–260. [[CrossRef](#)]
29. Enloe, C.M.; Findley, K.O.; Parish, C.M.; Miller, M.K.; DeCooman, B.C.; Speer, J.G. Compositional evolution of microalloy carbonitrides in a Mo-bearing microalloyed steel. *Scr. Mater.* **2013**, *68*, 55–58. [[CrossRef](#)]
30. Wang, Z.Q.; Zhang, H.; Guo, C.H.; Liu, W.B.; Yang, Z.G.; Sun, X.J.; Zhang, Z.Y.; Jiang, F.C. Effect of molybdenum addition on the precipitation of carbides in the austenite matrix of titanium micro-alloyed steels. *J. Mater. Sci.* **2016**, *51*, 4996–5007. [[CrossRef](#)]
31. Chijiwa, R.; Yoshida, Y.; Uemori, R.; Tamehiro, H.; Funato, K.; Horii, Y. Development and practical application of fire-resistant steel for buildings. *Nippon Steel Tech. Rep.* **1993**, *58*, 47–55.
32. Zhang, Z.Y.; Sun, X.J.; Wang, Z.Q.; Li, Z.D.; Yong, Q.L.; Wang, G.D. Carbide precipitation in austenite of Nb-Mo-bearing low-carbon steel during stress relaxation. *Mater. Lett.* **2015**, *159*, 249–252. [[CrossRef](#)]
33. Cao, Y.B.; Xiao, F.R.; Qiao, G.Y.; Huang, C.J.; Zhang, X.B.; Wu, Z.X.; Liao, B. Strain-induced precipitation and softening behaviors of high Nb microalloyed steels. *Sci. Eng. A* **2012**, *552*, 502–513. [[CrossRef](#)]

Disclaimer/Publisher’s Note: The statements, opinions and data contained in all publications are solely those of the individual author(s) and contributor(s) and not of MDPI and/or the editor(s). MDPI and/or the editor(s) disclaim responsibility for any injury to people or property resulting from any ideas, methods, instructions or products referred to in the content.